

## Article

# Experimental and Numerical Investigation of Hygrothermal Transfer through Bio-Based Materials: An Application to Wood–Cement Walls

Amer Bakkour <sup>1</sup>, Salah-Eddine Ouldboukhitine <sup>1,\*</sup>, Pascal Biwole <sup>1,2</sup>, Gael Godi <sup>1</sup> and Sofiane Amziane <sup>1</sup>

<sup>1</sup> Institut Pascal, Université Clermont Auvergne, CNRS, INP Clermont Auvergne, 63000 Clermont-Ferrand, France; amer.bakkour.95@gmail.com (A.B.); pascal.biwole@uca.fr (P.B.); gael.godi@uca.fr (G.G.); sofiane.amziane@uca.fr (S.A.)

<sup>2</sup> MINES Paris, PSL Research University, PERSEE-Center for Processes, Renewable Energies and Energy Systems, 06904 Sophia Antipolis, France

\* Correspondence: salah\_eddine.oudboukhitine@uca.fr

**Abstract:** In the context of the energy transition, new construction materials are emerging, notably bio-based materials such as wood concrete. This paper investigates the hygrothermal performance of walls constructed with wood–cement concrete. First, the thermal properties of wooden concrete, namely thermal conductivity, effusivity, and diffusivity, are experimentally characterized in both dry and wet conditions. Second, in situ measurements are carried out on a house in Lyon, a city in France, constructed with mono-layered wood–cement walls. This involves monitoring the temperature and relative humidity levels both inside and outside the building, as well as at three distinct positions within the wood walls over a 6-month period (from 20 April 2023 to 20 October 2023). The hygrothermal analysis at the center of the wall reveals that the wood wall effectively moderates fluctuations in the external temperature and relative humidity. Following this, a numerical study is performed to check the reliability of the adopted Reduced Heat, Air, and Mass (HAM) model to reproduce the hygrothermal performance of the wood–cement wall. The results show a strong agreement between the simulated and measured data, confirming the applicability of the ‘Reduced HAM’ model for the prediction of the hygrothermal behavior of wood–cement walls.

**Keywords:** bio-based material; heat and mass transfer; modeling; simulation; experimental characterization; wood–cement concrete



**Citation:** Bakkour, A.; Ouldboukhitine, S.-E.; Biwole, P.; Godi, G.; Amziane, S. Experimental and Numerical Investigation of Hygrothermal Transfer through Bio-Based Materials: An Application to Wood–Cement Walls. *Buildings* **2023**, *13*, 2986. <https://doi.org/10.3390/buildings13122986>

Academic Editor: Karim Ghazi Wakili

Received: 9 November 2023

Revised: 23 November 2023

Accepted: 28 November 2023

Published: 29 November 2023



**Copyright:** © 2023 by the authors. Licensee MDPI, Basel, Switzerland. This article is an open access article distributed under the terms and conditions of the Creative Commons Attribution (CC BY) license (<https://creativecommons.org/licenses/by/4.0/>).

## 1. Introduction

Great efforts are currently directed toward minimizing energy consumption in buildings and enhancing indoor air quality by incorporating construction materials with high hygrothermal performance. Bio-based materials show great promise for innovative and efficient solutions. They have the potential to significantly reduce energy consumption in buildings thanks to their low thermal conductivity and high thermal inertia. Additionally, these materials exhibit the capability to regulate both indoor temperature and relative humidity, providing enhanced hygrothermal comfort for occupants [1]. Notable examples of bio-based construction materials commonly used in this context include hemp [2], straw [3], date palm [4], sunflower [5], and flax [6].

Hygrothermal models are commonly used to describe the dynamics of heat and mass transfer within bio-based building envelopes, including walls, roofs, etc. The integration of these models into simulation tools equips designers with the capability to predict the evolution of temperature and relative humidity within a building assembly over time. This analysis enhances the comprehension of how the building envelope responds to both interior and exterior conditions and can help identify potential risks, such as condensation and mold growth.

### 1.1. Wood-Based Concretes

Wood-based concrete is part of a rapidly growing category of eco-friendly bio-based materials. Numerous studies have incorporated wood into concrete in various forms. These forms include using wood shavings as aggregates [7], incorporating wood waste (like sawdust and shavings) as partial or complete substitutes for conventional aggregates [8], and utilizing wood ash powder as cement replacement material [9].

For instance, Bederina et al. [10] examined the impact of adding wood shavings, the waste from woodworking activities, to sand-based concrete on thermal conductivity and mechanical performance. The results demonstrated that incorporating shavings into the sand-based concrete reduced material density and improved thermal efficiency. However, it also reduced the mechanical strength of the concrete.

Furthermore, other researchers have investigated the influence of the proportion of wood aggregates on the thermal and mechanical performance of clay–cement–wood composites [11]. The addition of wood aggregates to clayey concrete improves the insulation properties of these materials, but it resulted in a decrease in mechanical strength as the density decreased. Moreover, the moisture properties of lightweight concrete, comprised of clay, cement, and wood aggregates, were studied in [12], showing that the sorption–desorption isotherm curves of mixtures with varying percentages of wood aggregates exhibited a strong hysteresis.

Additional research has demonstrated that the thermal conductivity of concrete mixes can be reduced by incorporating wood waste [13–16]. Moreover, Ahmed et al. [17] recommended the use of sawdust-based concrete to improve the energy efficiency of buildings. The findings showed a 21.4% reduction in energy consumption related to the cooling load, thanks to the superior insulating properties of sawdust-based concrete. Moreover, a 13% reduction in CO<sub>2</sub> emissions was observed in a room constructed with sawdust concrete compared to conventional concrete. Recently, Alabduljabbar et al. [18] found that replacing the natural aggregates, including river sand and gravel, with sawdust waste offers competitive thermal and mechanical properties at an economical cost compared to other construction materials.

Limited research exists regarding the creation of lightweight composites using only wood aggregates combined with a cement binder. In the study of [19], the performance of a mixture of wood aggregates with water and cement was investigated primarily in terms of its elastic behavior. Similarly, Li et al. [7] examined the mechanical properties of wood–cement composites, although a small proportion of sand was introduced into the concrete formulation. In the study of [20], the thermal conductivity of the wood aggregate–cement composition was measured using the hot wire method. The findings revealed that the thermal conductivity of the wood composite is in the order of  $0.18 \text{ W}\cdot\text{m}^{-1}\cdot\text{K}^{-1}$ . Finally, Mnasri et al. [21] investigated the hygrothermal characteristics of a panel fabricated using wood chips, which constituted 89% of the panel's total volume, in combination with cement. The results revealed that the wood–cement composite exhibits an excellent moisture regulation capacity, with a moisture buffer value superior to  $3.0 \text{ (g/m}^2\cdot\% \text{ RH)}$ , and possesses a notable heat capacity of  $2.1 \text{ kJ}\cdot\text{kg}^{-1}\cdot\text{K}^{-1}$ .

The existing literature has highlighted that wood is a practical choice as a raw material for creating sustainable, lightweight concrete materials in construction. These mixed concretes have been extensively studied regarding their thermal and mechanical properties. Nevertheless, there is a scarcity of research concerning lightweight composites made only with a combination of wood aggregates combined with a cement binder. The wood-based concrete examined in this study is made with a mixture comprising water, wood aggregates sourced from certified French PEFC forestry operators, and cement as a binder that provides strength and durability. This wood–cement concrete contains 80% wood as a volume additive, with the remaining 20% being Ordinary Portland Cement.

### 1.2. Coupled Heat and Moisture Transfer: A Literature Review

In the field of building physics, hygrothermal models are extensively used to simulate the combined heat and moisture transfer within porous structures. The modeling of heat and moisture transfer has garnered considerable attention over several decades, starting with the foundational works of Philip and De Vries [22] in soil structures, followed by the contributions of Luikov [23]. These models have been developed based on the principles of heat and mass conservation, Fourier's law for heat conduction, and Fick's and Darcy's laws for gas and fluid diffusion.

Kunzel [24] developed, in 1995, a typical model for predicting the simultaneous heat and mass transfer within building components, using relative humidity and temperature as the driving potentials for moisture and heat, respectively. This model has found extensive use among researchers for assessing the hygrothermal behavior of various bio-based building walls [3,25,26]. Subsequently, numerous distinct numerical models have emerged. Depending on the chosen driving potentials, the coupled equations vary from one model to another, even when using common driving factors. Temperature is frequently employed as the driving potential for heat transfer. Conversely, with regard to mass transfer, various moisture-driving factors come into play, including vapor pressure, water content, and relative humidity. The following papers provide examples of research conducted in this area: Mendes et al. [27], Tariku et al. [28], Qin et al. (2009) [29], Van Belleghem et al. [30], Seng et al. [31], and Ferroukhi et al. [32].

Nevertheless, the lack of knowledge regarding the intrinsic characteristics of porous materials, coupled with the large number of input parameters that are often challenging to measure, either analytically or experimentally, poses a significant obstacle to the implementation of such models. This challenge has led some researchers to conduct a parametric sensitivity study of the hygrothermal models to investigate the influence of parameters on heat and mass transfer [33–36]. At the material scale, Benkhaled et al. [33] conducted a sensitivity analysis to identify the most influential parameters affecting hygrothermal transfer in hemp concrete. The study was based on the probability density distribution of bounded Gaussian law using MATLAB R2020a software. As a result, a simplified HAM model was elaborated by eliminating parameters that had minimal impact on the hygrothermal behavior of the material under investigation.

### 1.3. Aim of the Study

This study seeks to gain a deeper insight into the hygrothermal performance of wood–cement walls. The coupling of heat and moisture transfer within porous walls can significantly influence wall behavior as well as indoor air temperature and humidity. The existing simulation models for bio-based composites are complex for practical use.

In this study, we adopt the 'Reduced Heat, Air, and Mass' transfer model elaborated by Benkhaled et al. [33] through a parametric sensitivity analysis. Our goal is to assess the model's suitability in replicating temperature and relative humidity variations within wood–cement walls. To achieve this, we conduct a case study on a building constructed with wood–cement walls, where we measure the evolution of temperature and relative humidity at the exterior, interior, and within the walls. The simulated results obtained with the Reduced HAM model are then compared with the measured data. Given the lack of thermal properties of wood–cement concrete in the existing literature, we perform in-laboratory experimental characterization to determine the density and various thermal properties of this wood-based concrete.

In summary, the main objectives of this study are as follows:

- Determine the thermal properties of a concrete made from wood aggregates and cement.
- Conduct in situ measurements on a wood–cement building over a period of 6 months (from 20 April 2023 to 20 October 2023).
- Investigate the hygrothermal performance of hygroscopic wood–cement envelopes.
- Assess the reliability of the Reduced HAM model in predicting the hygrothermal performance of wood–cement walls.

Fulfilling these objectives will enable us to predict the hygrothermal behavior of wood–cement walls for different climates in the future work.

## 2. Laboratory Investigations

### 2.1. Characterization of the Thermal Properties of Wood Aggregate–Cement Concrete

In this study, a total of six specimens were prepared and tested. The wood concrete used in this examination is a mixture consisting of water, wood aggregates representing 80% of the concrete's volume, and Ordinary Portland Cement of the type CEM I 42.5R. The aggregates were pre-impregnated with the same cement to enhance the aggregate–cement adhesion and reduce the natural water absorption rate of the aggregates.

The specimens were divided into two groups based on their geometry dimensions (length, width, and height) (cm): Group 1 consisted of cubic specimens with dimension of (14.9, 14.9, 14.9) cm, while Group 2 comprised parallelepipedal specimens with dimension of (14.9, 14.9, 4.8) cm, as illustrated in Figure 1. The reason behind choosing different shapes lies in the fact that sample size can introduce variations in the measured intrinsic properties. Consequently, conducting measurements with different sample shapes contributes to achieving more precise and reliable results.

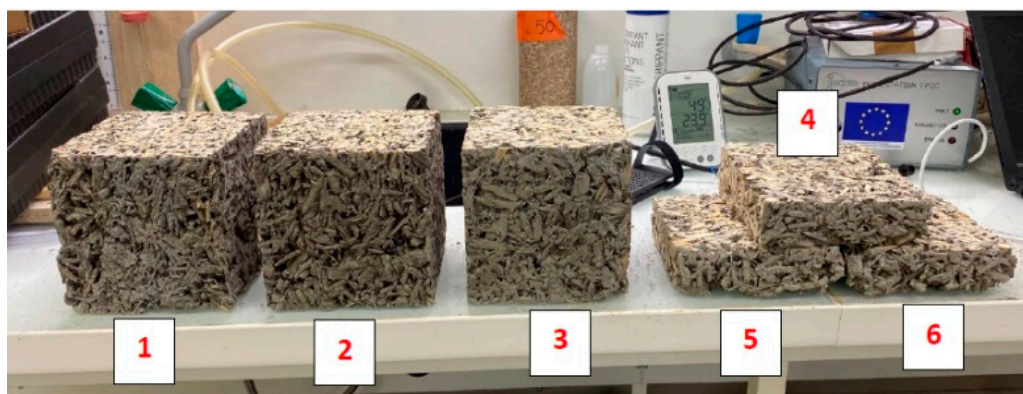


**Figure 1.** Cubic and parallelepipedal wood–cement composites.

The thermal properties of wood–cement composites were measured under both wet and dry conditions. For the wet test, specimens were maintained at a constant relative humidity of around 40% and a temperature of 22 °C in an air-conditioned room, as indicated by the digital hygro-thermometer. In contrast, to measure their properties in a dry state, the specimens were conditioned at 50 °C with an ambient humidity of 5% over a 3-day period using a dry chamber.

To measure the thermal conductivity, diffusivity, and thermal effusivity of wood–cement specimens, the NeoTIM-FP2C device, manufactured by the French-based company NeoTIM with measurement accuracy of 5%, was used (Figure 2). This device relies on the following:

- The hot wire method for measuring thermal conductivity.
- The hot ring method for measuring thermal diffusivity.
- The hot plane method for measuring thermal effusivity.

The method employed to measure the diverse thermal properties of the wood specimens involves inserting the appropriate “hot probe” between two samples. To ensure accuracy, the measurement was repeated multiple times to attain the most precise value for each thermal property. A summary of the total tests conducted under both wet and dry conditions is presented in Table 1.

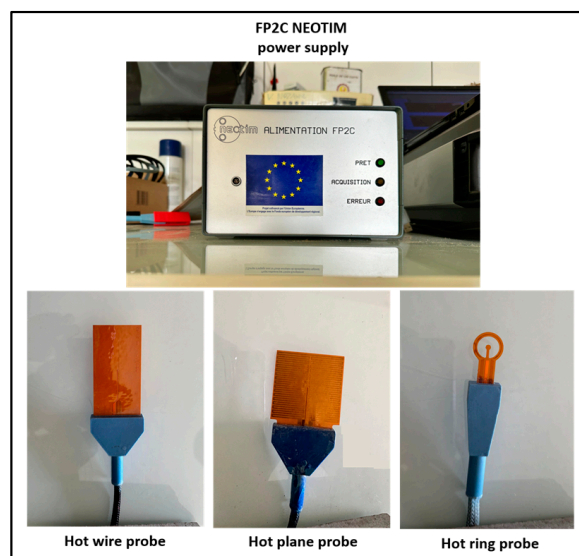


**Figure 2.** NeoTIM-FP2C device used for thermal characterization.

**Table 1.** Number of measurement tests applied on wood specimens.

Conditions		Thermal Conductivity	Thermal Effusivity	Thermal Diffusivity
Wet	Cubic	24	24	24
	Parallelepipedal	24	12	16
Dry	Cubic	24	24	24
	Parallelepipedal	20	14	16

The specimens were weighted using a digital scale to calculate their apparent density.

## 2.2. Experimental Results

Table 2 gives the mean and standard deviation of the thermal conductivity, effusivity, and thermal diffusivity of the studied materials. There is a slight disparity in values between the different shapes of wood–cement specimens, with cubic forms consistently exhibiting higher values than parallelepipedal shapes. Additionally, it is evident that the thermal performance of the cementitious composites decreases in the wet condition.

**Table 2.** Thermal properties of wood aggregate–cement composites.

Thermal Properties	Wet Condition		Dry Condition	
	Cubic	Parallelepipedal	Cubic	Parallelepipedal
Thermal conductivity ( $W \cdot m^{-1} \cdot K^{-1}$ )	$0.146 \pm 0.017$	$0.129 \pm 0.018$	$0.132 \pm 0.027$	$0.118 \pm 0.021$
Thermal effusivity ( $J \cdot m^{-2} \cdot K^{-1} \cdot s^{-1/2}$ )	$303 \pm 44$	$276 \pm 41$	$266 \pm 45$	$248 \pm 28$
Thermal diffusivity ( $m^2 \cdot s^{-1}$ ) ( $\times 10^{-7}$ )	$4.42 \pm 0.43$	$3.70 \pm 0.56$	$3.72 \pm 0.67$	$3.37 \pm 0.50$

In wet conditions, the average values for thermal conductivity, effusivity, and diffusivity between cubic and parallelepipedal shapes are  $0.137 \pm 0.019$  ( $W \cdot m^{-1} \cdot K^{-1}$ ),  $294 \pm 44$  ( $J \cdot m^{-2} \cdot K^{-1} \cdot s^{-1/2}$ ), and  $4.13 \pm 0.60 \times 10^{-7}$  ( $m^2 \cdot s^{-1}$ ), respectively. For dry conditions, the average value are  $0.126 \pm 0.025$  ( $W \cdot m^{-1} \cdot K^{-1}$ ),  $259 \pm 40$  ( $J \cdot m^{-2} \cdot K^{-1} \cdot s^{-1/2}$ ), and  $3.58 \pm 0.62 \times 10^{-7}$  ( $m^2 \cdot s^{-1}$ ) for thermal conductivity, effusivity, and diffusivity, respectively.

The thermal conductivity value closely aligns with that of the clay–cement–wood composite described in [11], which records a thermal conductivity of  $0.14 \text{ (W}\cdot\text{m}^{-1}\cdot\text{K}^{-1})$  and a material density of  $700 \text{ kg}\cdot\text{m}^{-3}$  when the concrete formulation includes a 40% weight percentage of wood aggregates.

### 3. In Situ Investigations of the Hygrothermal Performance of Wood–Cement Walls

This study primarily focuses on the evolution of temperature and relative humidity within wood–cement walls. The building under investigation is constructed using prefabricated envelopes made of wood–cement concretes, with reinforced concrete posts regularly installed within the structure. The building is a single-floor structure situated in Lyon, in the southeast of France, covering an area of approximately  $212 \text{ m}^2$ , as shown in Figure 3. Its envelope is 30 cm thick, with the internal surface coated with paint and the external surface covered with plaster. The building is equipped with an HVAC system to regulate the indoor temperature and relative humidity and ensure indoor comfort. Additionally, a weather station was installed a few meters away from the building to measure the outdoor weather conditions. The weather in Lyon is characterized as temperate, as indicated in Figure 4.

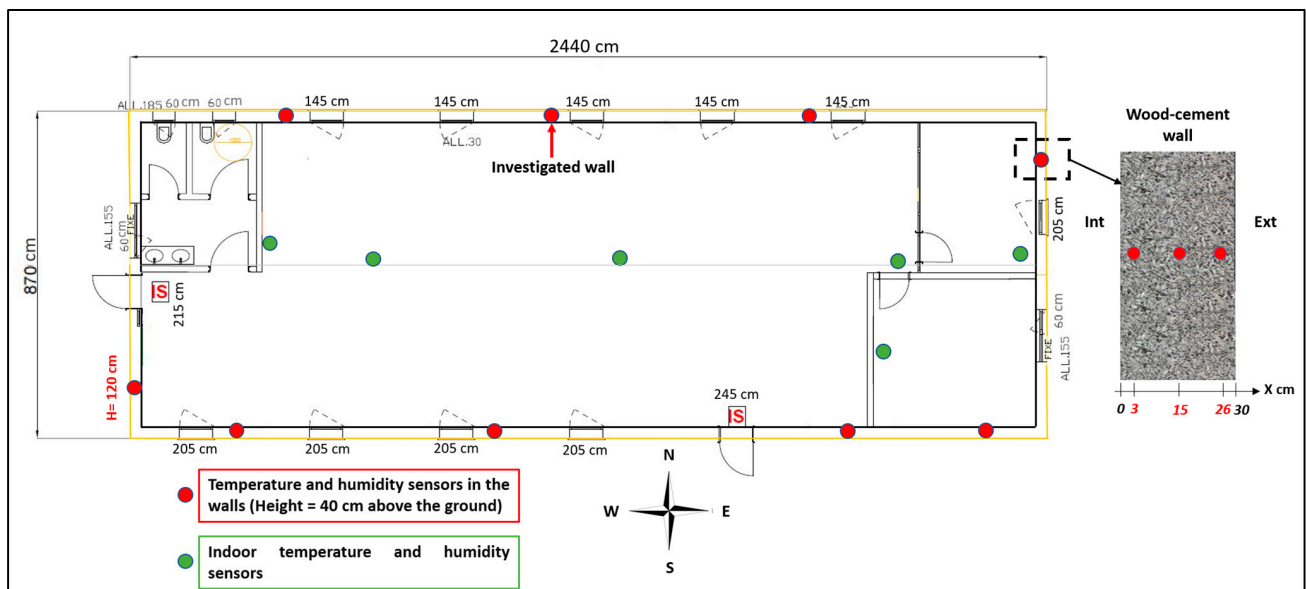


Figure 3. Drawing plan of the investigated wood–cement building located in Lyon, France.

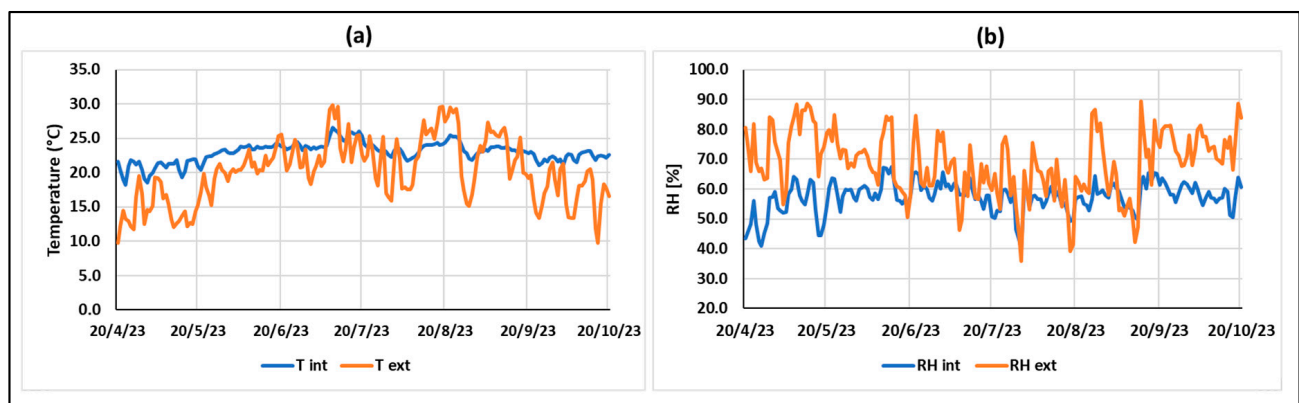


Figure 4. Daily variations in indoor and outdoor temperature (a) and relative humidity (b).

To evaluate the hygrothermal performance of the wood-based building, monitoring campaigns were carried out for indoor hygrothermal conditions, as well as within the wood walls at three different positions (3 cm from interior side, at the center of the wall, and

4 cm from the exterior side). These campaigns span a 6-month period, from 20 April 2023, to 20 October 2023. Figure 4 illustrates the daily fluctuations in indoor and outdoor air temperature and relative humidity during this timeframe. While the data were continuously recorded at hourly intervals, daily averages are considered for better data visualization.

Since the investigated building is equipped with an HVAC system, the indoor temperature and relative humidity remain quite stable despite the high fluctuations in outdoor conditions. Indoor temperature varies between 20 °C and 26 °C, while indoor relative humidity ranges from 40% to 65%. These levels fall within the comfort range recommended by the international standard NF EN 16798-1 [37]. For Category II office spaces, the standard recommends an indoor temperature range of 20–24 °C and a relative humidity of about 40% in the winter, and a temperature range of 23–26 °C with a relative humidity of about 60% in the summer.

One of the objectives of the experimental measurement campaign is to assess the insulation effectiveness and humidity regulation capability of wood–cement envelopes. As previously mentioned, hygrothermal sensors are positioned in three different locations within the building’s walls. However, given that the indoor environment is controlled by a heating/cooling system, the investigation of the wood walls’ response at the central position is considered more reliable, as the interior position is influenced by indoor conditions. Figure 5 compares the temperature and relative humidity variations at the center of the wall with indoor and outdoor conditions. Because of data acquisition errors in some walls during this period, the northern wall was selected for this study.

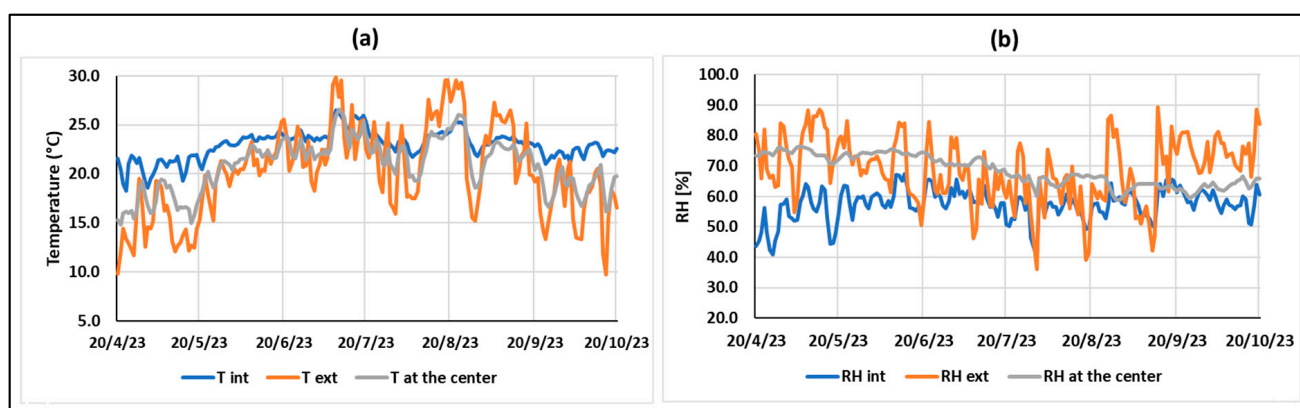


**Figure 5.** Hygrothermal response at the central position: temperature (a) and relative humidity (b) of the wood–cement wall.

From a thermal viewpoint, the insulating property of the wood wall is demonstrated by the temperature difference between the outdoor environment and the central position of the wall during the winter. On April 20 and October 16, the daily average outdoor temperature dropped to 10 °C, while the temperature at the middle of the wall was around 15 °C. The walls exhibited the ability to increase the minimal outdoor temperatures by 50%.

From a hydric viewpoint, despite the significant values of outdoor relative humidity, the relative humidity values at the center of the wall remained relatively stable, with daily average RH ranging between 60% and 75%. The wall demonstrated the capability to mitigate outdoor RH fluctuations. This behavior can be attributed to the wood concrete’s effective moisture buffering properties, which involve an exchange of moisture with the surroundings.

These results indicate that the building envelope can effectively control external temperature and relative humidity extremes, thereby enhancing indoor comfort.

To further explore the hygrothermal aspects, we are examining two crucial factors that play a pivotal role in enhancing the indoor thermal performance of buildings: Time Lag ( $\phi$ ) and Decrement Factor ( $DF$ ). These two thermal inertia parameters hold significant importance in the analysis and interpretation of a building envelope’s heat storage capabilities.

Time Lag refers to the duration it takes for a heat wave to propagate from the outer surface to the inner surface of the building, while the decreasing ratio of its amplitude during this process is defined as the Decrement Factor. These two parameters are mathematically expressed in Equations (1) and (2). Building envelopes with high time lags and small decrement factors contribute to an improved indoor thermal comfort level.

$$\phi = t_{T_i, \max} - t_{T_e, \max} \quad (1)$$

$$DF = \frac{T_{i, \max} - T_{i, \min}}{T_{e, \max} - T_{e, \min}} \quad (2)$$

where  $t_{T_i, \max}$  and  $t_{T_e, \max}$  are the times when the inside and outside temperatures are at their maximum, and  $T_{i, \max}$ ,  $T_{i, \min}$ ,  $T_{e, \max}$ , and  $T_{e, \min}$  represent the maximum and minimum temperatures of both the internal and external surfaces.

As we are focusing on the central position of the wall, the indoor temperature mentioned in Equations (1) and (2) will be substituted with the temperature at the wall's center. Consequently, this study focuses on the time it takes for the heat wave to travel from the outer surface to the center of the wall along with the decreasing ratio of its amplitude. Figure 6 illustrates the evolution of outdoor and central temperatures for the Northern wall on 22nd August, where the external temperature reaches its maximum magnitude of 38.1 °C.

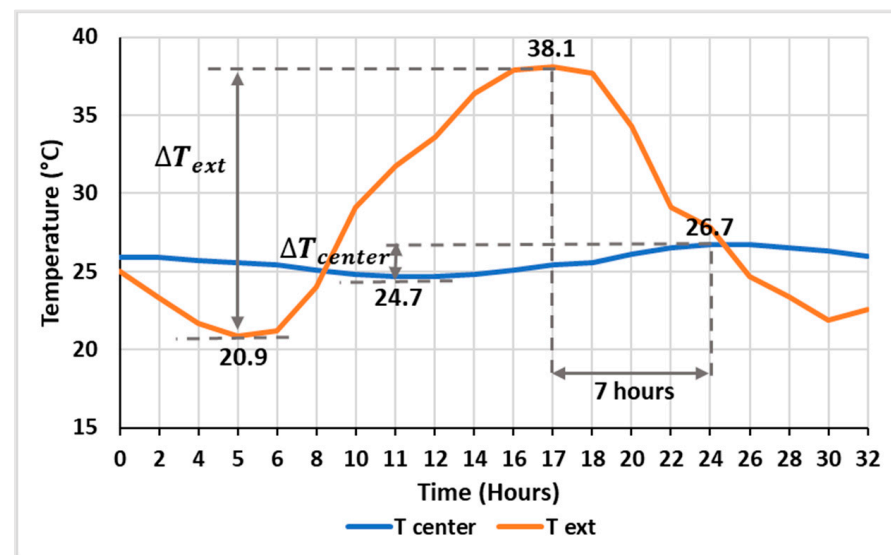


**Figure 6.** Evolution of outdoor temperature and the temperature at the wall's center: detail on the 22 August 2023.

Figure 6 highlights a phase shift of approximately 7 h and a heat flow damping rate of about 11.6%. Thanks to the good thermal inertia of the wood–cement wall, the temperature peak at the center of the wall occurs as the external temperatures decrease, particularly during the night. This phenomenon helps mitigate overheating during the summer. It is worth noting that these two factors depend on several factors, including thermophysical properties and wall thickness [38], as well as building outside temperatures [39].

Additionally, it is crucial to analyze the temperature trends of the northern wall in comparison to other orientations. This comparative analysis focuses on the temperature at a specific location, positioned 4 cm from the exterior. It particularly examines the contrast between the northern and southern walls over two distinct months, namely May and August, as illustrated in Figure 7. Notably, it becomes apparent that the southern wall consistently registers higher temperatures than its northern wall throughout the observed duration. This disparity can be attributed to several factors that influence thermal dynamics.

The southern wall, due to its orientation, is more exposed to direct sunlight, leading to the absorption and prolonged retention of heat. The higher angle of the sun in the sky during the day, coupled with a favorable sun path, results in increased solar exposure on the southern wall, consequently maintaining elevated temperatures. Conversely, the northern wall, positioned in the shadow of the building, receives less direct sunlight, leading to diminished solar heating, and subsequently, lower temperatures. These consistent temperature variations underscore the significant impact of orientation and solar exposure on the thermal behavior of the building throughout the changing seasons, highlighting the importance of considering these factors in the overall assessment and design of structures for optimal thermal performance.

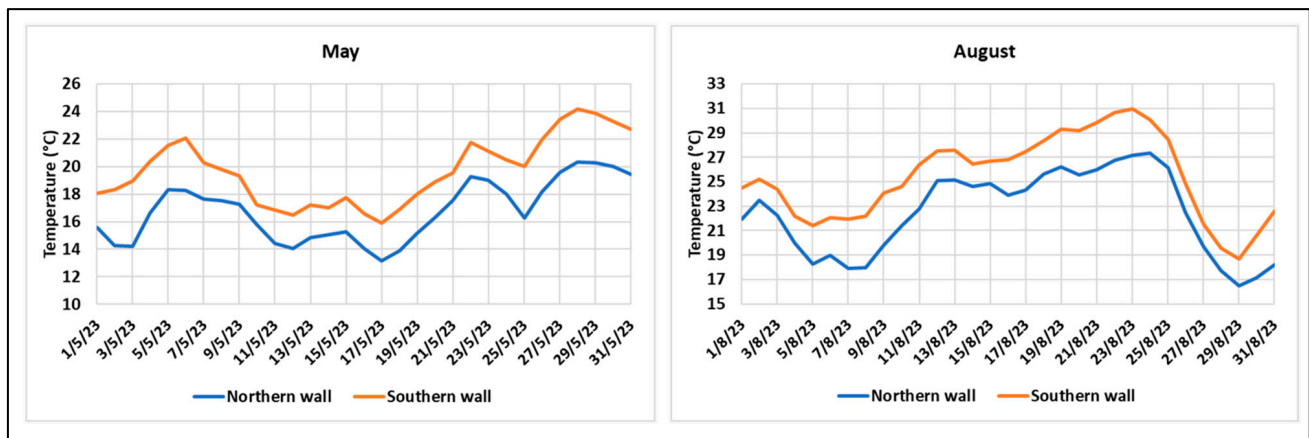


**Figure 7.** Daily temperature trends at a position 4 cm from exterior wall surface for the northern and southern walls.

## 4. Simulation of the Hygrothermal Behavior of Wood–Cement Wall

### 4.1. Numerical Model

In this study, the Reduced Heat, Air, and Mass (HAM) transfer model elaborated by [33] is adopted. The Reduced HAM model was the fruit of a parametric sensitivity analysis that aimed to establish correlations between the hygrothermal parameters of hemp concrete and the driving transfer potentials (temperature  $T$ , vapor pressure  $P_v$ , and total pressure  $P$ ). The most influential parameters (thermal conductivity  $\lambda$ , specific heat  $C_p$ , water storage capacity  $C_m$ , and water vapor permeability  $K_m$ ) were identified, and the less influential ones were eliminated. The simplified HAM model is described as follows:

$$C_p \rho_s \frac{\partial T}{\partial t} = \text{div}[\lambda \nabla T] + L_v \rho_s C_m \frac{\partial P_v}{\partial t} \quad (3)$$

$$\rho_s C_m \frac{\partial P_v}{\partial t} = \text{div}[K_m \nabla P_v] \quad (4)$$

where  $C_p$  ( $\text{J} \cdot \text{kg}^{-1} \cdot \text{K}^{-1}$ ) the specific heat capacity,  $\rho_s$  ( $\text{kg} \cdot \text{m}^{-3}$ ) the density,  $\lambda$  ( $\text{W} \cdot \text{m}^{-1} \cdot \text{K}^{-1}$ ) the thermal conductivity,  $L_v = 2.5 \times 10^6$  ( $\text{J} \cdot \text{kg}^{-1}$ ) the latent heat,  $C_m = \left(\frac{\partial \omega}{\partial \varphi}\right) \left(\frac{1}{P_{vsat}}\right)$  ( $\text{kg} \cdot \text{kg}^{-1} \cdot \text{Pa}^{-1}$ ) the moisture storage capacity,  $\varphi$  (%) the relative humidity,  $\omega$  ( $\text{kg} \cdot \text{kg}^{-1}$ ) the water content within the material, and  $K_m$  ( $\text{kg} \cdot \text{m}^{-1} \cdot \text{s}^{-1} \cdot \text{Pa}^{-1}$ ) the total moisture permeability.

As demonstrated by [33], the model showed strong accuracy in its application to bio-based hemp concrete. The objective is to confirm its reliability in simulating the hygrothermal performance of wood–cement walls under real outdoor conditions.

Under identical temperature conditions, relative humidity is defined as the ratio of the water vapor pressure  $P_v$  to the saturated water vapor pressure  $P_{vsat}$ :

$$RH = P_v / P_{vsat} \quad (5)$$

The temperature dependence of the saturation vapor pressure is illustrated with the following empirical expression, valid for  $0\text{ }^{\circ}\text{C} < T < 80\text{ }^{\circ}\text{C}$  with an accuracy of 0.15% [40]:

$$P_{\text{vsat}} = \exp\left(23.5771 - \frac{4042.9}{T - 37.58}\right) \quad (6)$$

with  $T$  is expressed in Kelvin (K).

#### 4.2. Input Data for Hygrothermal Simulation

The thermal properties characterized in the previous section offer valuable data for model validation. We consider the average value between cubic and parallelepipedal shapes under wet conditions. The heat capacity ( $C_p$ ) was derived from thermal conductivity and effusivity using the formula  $E = \sqrt{\rho \cdot C_p \cdot \lambda}$ .

As there is limited information on the water vapor permeability and water storage capacity of wood aggregate–cement concrete in the literature, these parameters are estimated. The values of water sorption capacity  $C_m$  and the water vapor permeability  $K_m$  are assumed to be the same as those used in the numerical study conducted by [33], which addresses hygrothermal simulations within bio-based concrete. Table 3 summarizes the input hygrothermal parameters used in this numerical validation.

**Table 3.** Input parameters for wood–cement concrete used in the numerical validation.

$\rho_s$ ( $\text{kg}\cdot\text{m}^{-3}$ )	$\lambda$ ( $\text{W}\cdot\text{m}^{-1}\cdot\text{K}^{-1}$ )	$C_p$ ( $\text{J}\cdot\text{kg}^{-1}\cdot\text{K}^{-1}$ )	$C_m$ ( $\text{kg}\cdot\text{kg}^{-1}\cdot\text{Pa}^{-1}$ )	$K_m$ ( $\text{kg}\cdot\text{m}^{-1}\cdot\text{s}^{-1}\cdot\text{Pa}^{-1}$ )
612	0.14	1007	$3.7 \times 10^{-6}$	$6 \times 10^{-10}$

#### 4.3. Initial Conditions

Predicting the hygrothermal performance of a building envelope typically relies on knowledge of the enclosure’s geometry, material properties, boundary conditions, and initial conditions. Since the distribution of initial conditions within the wall is often unknown, the simulation’s starting points are estimated based on the boundary conditions at the internal and external surfaces of the wall. In this study, we assumed that the initial temperature ( $T_0$ ) and relative humidity ( $RH_0$ ) vary linearly along the wall, as described in Equations (7) and (8). The transition occurs gradually from the internal conditions at one end of the wall ( $T_0(x=0) = T_i$  and  $RH_0(x=0) = RH_i$ ) to the external conditions at the other end ( $T_0(x=L) = T_e$  and  $RH_0(x=L) = RH_e$ ).

$$T_0(x) = T_{\text{surface},i} + \frac{(T_{\text{surface},e} - T_{\text{surface},i})}{L} \cdot x \quad (7)$$

$$RH_0(x) = RH_{\text{surface},i} + \frac{(RH_{\text{surface},e} - RH_{\text{surface},i})}{L} \cdot x \quad (8)$$

where  $L$  represents the length of the wall,  $x$  is the position within the wall,  $T_{\text{surface},i}$  and  $T_{\text{surface},e}$  correspond to the temperature at the internal and external wall surfaces, respectively, and  $RH_{\text{surface},i}$  and  $RH_{\text{surface},e}$  denote the relative humidity at the internal and external wall surfaces.

#### 4.4. Boundary Conditions

The accuracy of a mathematical model is not only reliant on proper hygrothermal transfer modeling but also greatly influenced by the boundary conditions applied. Properly addressing the surface interactions at the boundaries between the building’s envelope and its surroundings is a key aspect of successful modeling. It involves the exchange of heat and mass between the surface and the adjacent air.

The external environment is typically characterized by various meteorological parameters, such as wind velocity, wind direction, ambient air pressure, and incident solar radiation. This is why the temperature and relative humidity measured outside by the

weather station may not precisely reflect the conditions immediately adjacent to the wall, especially when the weather station is positioned at a distance from the building. Therefore, modeling these phenomena can be quite complex.

To address the issue of setting boundary conditions at the external surface, a calibration method based on the measurements obtained from a sensor positioned within the wall at 4 cm from the exterior is employed. The calibration process involves considering a specified interval of temperature and relative humidity variations over time, as outlined below:

$$T_{surface, ext}(t) = T_{sensor\ 4cm\ from\ ext}(t) - [0.3\ 0.6] \text{ } ^\circ\text{C} \quad (9)$$

$$RH_{surface, ext}(t) = RH_{sensor\ 4cm\ from\ ext}(t) + [1\% \ 4\%] \quad (10)$$

Conversely, the indoor environment is characterized by temperature and relative humidity values. In this context, we applied Dirichlet conditions to the inner wall surface, setting the temperature and relative humidity equal to those of the indoor air.

#### 4.5. Numerical Simulation Tool: COMSOL Multiphysics

To solve the coupled equations related to the Reduced HAM model, the COMSOL Multiphysics v. 5.5 software was selected. This software provides a robust platform for modeling and solving a wide range of engineering and research problems. It is especially well-suited for handling Multiphysics problems where several phenomena are studied simultaneously, as is the case of heat and mass transfer. The software employs the finite element method for solving partial differential equations.

In COMSOL, the “Mathematics” branch is the optimal choice for solving equation-based models as it supports various formulations (weak form, general form, coefficient form PDE, etc.) of partial differential equations (PDEs). Within the “PDE interfaces”, the preferred equation formulation for entering the equations is the “Coefficient form PDE”. This formulation allows the specification of coefficients for well-known PDEs containing derivatives up to the second order in both time and space (Equation (11)). The user only needs to input the coefficients for the relevant equations. For a variable  $u$ , the PDE is expressed as follows:

$$e_a \frac{\partial^2 u}{\partial t^2} + d_a \frac{\partial u}{\partial t} + \nabla \cdot (-c \nabla u - \alpha u + \gamma) + \beta \cdot \nabla u + a u = f \quad (11)$$

where,  $e_a$  ( $\text{s}^2 \cdot \text{m}^{-2}$ ) is the mass coefficient,  $d_a$  ( $\text{s}^2 \cdot \text{m}^{-2}$ ) is the damping coefficient or mass coefficient,  $c$  (-) is the diffusion coefficient,  $\alpha$  ( $\text{m}^{-1}$ ) is the conservative flux convection coefficient,  $\gamma$  ( $\text{m}^{-1}$ ) is the conservative flux source,  $\beta$  ( $\text{m}^{-1}$ ) is the convection coefficient,  $a$  ( $\text{m}^{-2}$ ) is the absorption coefficient, and  $f$  ( $\text{m}^{-2}$ ) is the source term, as documented in the COMSOL Manual Reference [41] (p. 995).

In our case, the field vector  $u$  of the 1D Reduced HAM model is defined as a matrix of two independent transfer variables: temperature  $T$  and the vapor pressure  $P_v$ .

$$u = [T, P_v]^T \quad (12)$$

Comparing the heat and moisture balances defined in Equations (3) and (4) with COMSOL PDE equation form (Equation (11)), we can identify the non-zero coefficients of Equation (11). Assuming no internal heat sources and sinks, the non-zero values correspond to the diffusion and damping or mass coefficients ( $d_a$  and  $c$ ). The equation can then be simplified as follows:

$$d_a \frac{\partial u}{\partial t} + \nabla \cdot (-c \nabla u) = 0 \quad (13)$$

After making the necessary replacements, the “coefficient form PDE” will appear as follows:

$$\begin{bmatrix} C_p \cdot \rho_s & -L_v \cdot \rho_s \cdot C_m \\ 0 & \rho_s \cdot C_m \end{bmatrix} \begin{bmatrix} \frac{\partial T}{\partial t} \\ \frac{\partial P_v}{\partial t} \end{bmatrix} + \left( - \begin{bmatrix} \lambda & 0 \\ 0 & K_m \end{bmatrix} \cdot \nabla \begin{bmatrix} \nabla T \\ \nabla P_v \end{bmatrix} \right) = 0 \quad (14)$$

with  $d_a = \begin{bmatrix} C_p \cdot \rho_s & -L_v \cdot \rho_s \cdot C_m \\ 0 & \rho_s \cdot C_m \end{bmatrix}$  and  $c = \begin{bmatrix} \lambda & 0 \\ 0 & K_m \end{bmatrix}$ .

These coefficients form the equation used by COMSOL to determine the evolution of temperature, vapor pressure, and relative humidity inside the wood–cement wall.

The algorithm for implementing the Reduced HAM model in COMSOL Multiphysics is illustrated in Figure 8.

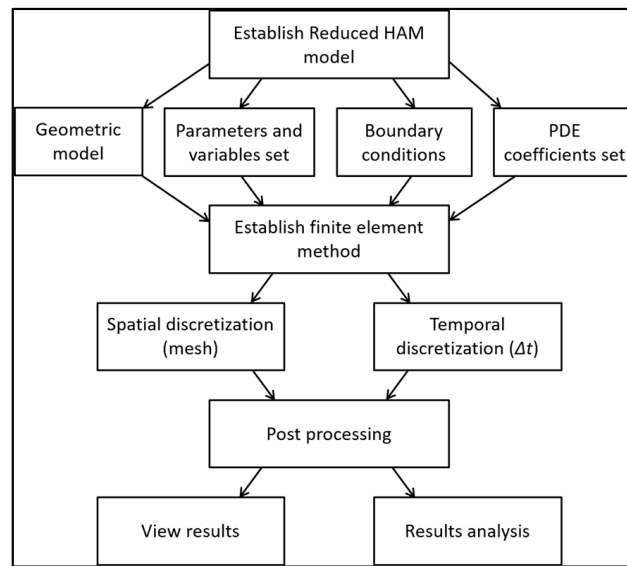


Figure 8. Flowchart of the algorithm for solving coupled HAM transfer equations with COMSOL.

#### 4.6. Simulation Results

The simulation is carried out with a number of nodes of 100 and a time step of 1 day. Figures 9 and 10 present the daily-averaged experimental and simulated results, showing the temperature and the RH at the three different position: 3 cm from the interior surface, 4 cm from the exterior surface, and the center of the northern wall.

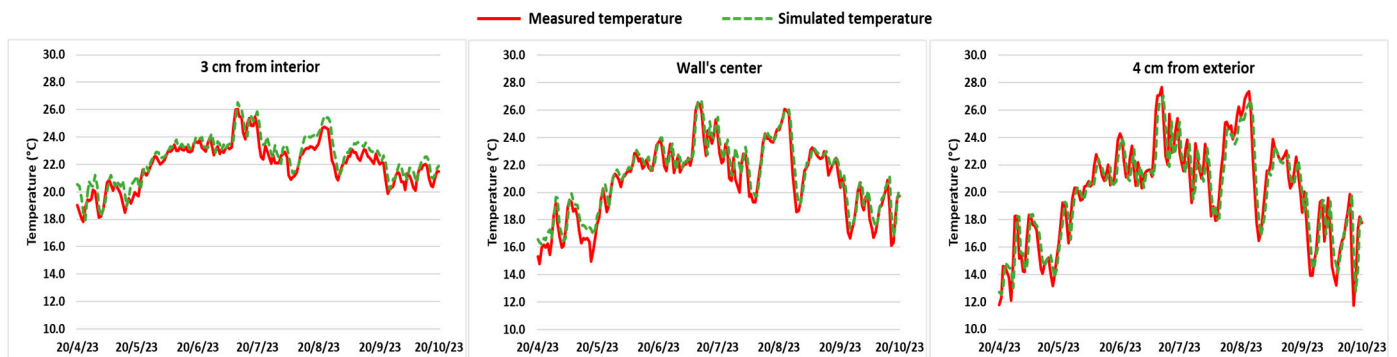
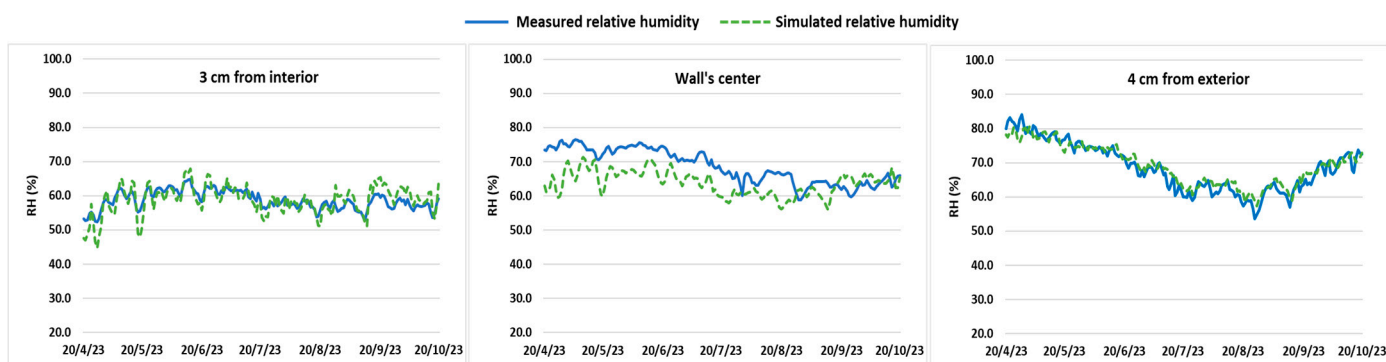


Figure 9. Comparison of temperature between the simulated and measured results for three different positions within the northern wall.



**Figure 10.** Comparison of relative humidity between the simulated and measured results for three different positions within the northern wall.

The Reduced HAM model implemented in COMSOL generates almost similar results as the in-situ measurements of the wood–cement building for the studied weather conditions. In terms of temperature, the plotted values agree well with the measured values at all three positions.

Furthermore, the RH variation within the wood wall closely matches the experimental results. The RH behavior at the interior and exterior positions in the wall closely corresponds to the in-situ measurements. However, a slight variation in the relative humidity values is observed at the center position. The assumed water vapor permeability and sorption capacity of the wood concrete implemented in the numerical model can account for the differences in RH variation at the center position.

To evaluate the agreement between experimental data and simulated outcomes, the root mean square error (*RMSE*) and the relative error (*RE*) are utilized, as defined in Equations (15) and (16).

$$RMSE = \sqrt{\frac{\sum_{i=1}^N (x_{i,m} - x_{i,e})^2}{N}} \tag{15}$$

$$RE = \frac{100}{N} \cdot \sum_{i=1}^n \frac{|x_{i,m} - x_{i,e}|}{x_{i,m}} \tag{16}$$

where  $x_m$  is the measured value,  $x_e$  is the estimated value using the model, and  $N$  is the total number of values.

The calculated relative error (*RE*) and the root mean square error (*RMSE*) for temperature and relative humidity are presented in Table 4. The *RE* and *RSME* for the interior surface temperature are 2.78% and 0.74 °C, respectively, while those for the exterior surface temperature are 5.82% and 1.41 °C, respectively. The *RE* and *RSME* for the interior surface RH are 3.93% and 2.79%, respectively, while those for the exterior surface RH are 2.66% and 2.25%. For the center of the wall, the temperature *RE* and *RSME* are 3.23% and 0.84 °C, respectively, while the relative humidity *RE* and *RSME* are 8% and 6.53%.

**Table 4.** The calculated relative error and the root mean square error.

Position in the Wall		Temperature (°C)	RH (%)
3 cm from the interior	<i>RE</i> (%)	2.78	3.95
	<i>RMSE</i>	0.74	2.80
Center	<i>RE</i> (%)	3.21	8.06
	<i>RMSE</i>	0.84	6.54
4 cm from the exterior	<i>RE</i> (%)	5.81	2.67
	<i>RMSE</i>	1.41	2.25

These values quantitatively demonstrate the strong agreement between the numerical and experimental models. The numerical model can, therefore, be utilized to predict the hygrothermal performance of the wood–cement walls.

## 5. Conclusions

This study evaluates the hygrothermal performance of walls constructed with wood–cement concrete. First, the thermal properties of concrete, which are created by combining water, wood aggregates that make up 80% of the concrete’s volume, and cement, are characterized. The results demonstrated that this type of concrete exhibits good insulation properties, indicated by low thermal conductivity and diffusivity ( $0.137 \pm 0.019$  ( $\text{W}\cdot\text{m}^{-1}\cdot\text{K}^{-1}$ ) and  $4.13 \pm 0.60 \times 10^{-7}$  ( $\text{m}^2\cdot\text{s}^{-1}$ ), respectively) under wet condition.

Subsequently, in situ measurements are conducted both inside and outside the building, as well as at various positions within the wood walls, over a 6-month period from 20 April 2023 to 20 October 2023. The hygrothermal analysis at the center of the wall reveals that the wood wall effectively moderates fluctuations in external temperature and relative humidity. This is evident through a phase shift of approximately 7 h and a heat flow damping rate of about 11.6%. The temperature peak at the center of the wall occurs as external temperatures decrease, particularly during the night.

Following this, a dynamic simulation of the wood–cement wall’s hygrothermal behavior is performed. The Reduced Heat, Air, and Mass (HAM) model, adopted in this study, is implemented in COMSOL and validated using experimental data. The comparison between numerical and measured results confirms the model’s ability to predict the hygrothermal performance of wood–cement walls.

After successfully validating the Reduced HAM Model at the scale of the wall, our future objective is to integrate this model with building energy simulation tools to achieve comprehensive hygrothermal modeling of buildings. This integration will allow us to predict the impact of bio-based materials on the overall energy demand of buildings, including potential reductions in both heating and cooling costs.

**Author Contributions:** Conceptualization, S.-E.O. and S.A.; methodology, S.-E.O. and S.A.; software, A.B. and S.-E.O.; validation, A.B. and S.-E.O.; formal analysis, A.B.; investigation, A.B.; resources, A.B. and G.G.; data curation, A.B. and G.G.; writing—original draft preparation, A.B. and S.-E.O.; writing—review and editing, S.-E.O., P.B. and A.B.; visualization, S.A. and S.-E.O.; supervision, S.A., P.B. and S.-E.O.; project administration, S.A.; funding acquisition, S.A. All authors have read and agreed to the published version of the manuscript.

**Funding:** This research was funded by the Allier General Council, France, project-ID: DRED-ED-HDR\_2022-073.

**Data Availability Statement:** Data are contained within the article.

**Conflicts of Interest:** The authors declare no conflict of interest.

## References

1. Bakkour, A.; Ouldboukhitine, S.-E.; Biwole, P.; Amziane, S. Assessing Hygrothermal Parameters of Plant-Based Building Materials for Simulation: A Mini Review. In *International Conference on Bio-Based Building Materials*; Springer Nature: Cham, Switzerland, 2023; pp. 450–464.
2. Maalouf, C.; Le, A.D.T.; Umurigirwa, S.B.; Lachi, M.; Douzane, O. Study of hygrothermal behaviour of a hemp concrete building envelope under summer conditions in France. *Energy Build.* **2014**, *77*, 48–57. [[CrossRef](#)]
3. Tlaji, G.; Pennec, F.; Ouldboukhitine, S.; Ibrahim, M.; Biwole, P. Hygrothermal performance of multilayer straw walls in different climates. *Constr. Build. Mater.* **2022**, *326*, 126873. [[CrossRef](#)]
4. Haba, B.; Agoudjil, B.; Boudenne, A.; Benzarti, K. Hygric properties and thermal conductivity of a new insulation material for building based on date palm concrete. *Constr. Build. Mater.* **2017**, *154*, 963–971. [[CrossRef](#)]
5. Abbas, M.S.; McGregor, F.; Fabbri, A.; Ferroukhi, M.Y. The use of pith in the formulation of lightweight bio-based composites: Impact on mechanical and hygrothermal properties. *Constr. Build. Mater.* **2020**, *259*, 120573. [[CrossRef](#)]
6. Rahim, M.; Douzane, O.; Tran Le, A.D.; Langlet, T. Effect of moisture and temperature on thermal properties of three bio-based materials. *Constr. Build. Mater.* **2016**, *111*, 119–127. [[CrossRef](#)]

7. Li, M.; Khelifa, M.; El Ganaoui, M. Mechanical characterization of concrete containing wood shavings as aggregates. *Int. J. Sustain. Built Environ.* **2017**, *6*, 587–596. [CrossRef]
8. Mohammed, B.S.; Abdullahi, M.; Hoong, C.K. Statistical models for concrete containing wood chipping as partial replacement to fine aggregate. *Constr. Build. Mater.* **2014**, *55*, 13–19. [CrossRef]
9. Elinwa, A.U.; Mahmood, Y.A. Ash from timber waste as cement replacement material. *Cem. Concr. Compos.* **2002**, *24*, 219–222. [CrossRef]
10. Bederina, M.; Marmoret, L.; Mezreb, K.; Khenfer, M.M.; Bali, A.; Quéneudec, M. Effect of the addition of wood shavings on thermal conductivity of sand concretes: Experimental study and modelling. *Constr. Build. Mater.* **2007**, *21*, 662–668. [CrossRef]
11. Al Rim, K.; Ledhem, A.; Douzane, O.; Dheilily, R.M.; Queneudec, M. Influence of the proportion of wood on the thermal and mechanical performances of clay-cement-wood composites. *Cem. Concr. Compos.* **1999**, *21*, 269–276. [CrossRef]
12. Bouguerra, A.; Sallée, H.; de Barquin, F.; Dheilily, R.M.; Quéneudec, M. Isothermal moisture properties of wood-cementitious composites. *Cem. Concr. Res.* **1999**, *29*, 339–347. [CrossRef]
13. Fu, Q.; Yan, L.; Ning, T.; Wang, B.; Kasal, B. Behavior of adhesively bonded engineered wood—Wood chip concrete composite decks: Experimental and analytical studies. *Constr. Build. Mater.* **2020**, *247*, 118578. [CrossRef]
14. Hafidh, S.A.; Abdullah, T.A.; Hashim, F.G.; Mohmoud, B.K. Effect of Adding Sawdust to Cement on its Thermal Conductivity and Compressive Strength. *IOP Conf. Ser. Mater. Sci. Eng.* **2021**, *1094*, 012047. [CrossRef]
15. Taoukil, D.; El Bouardi, A.; Ezbakhe, H.; Ajzoul, T. Thermal Properties of Concrete Lightened by Wood Aggregates. *Res. J. Appl. Sci. Eng. Technol.* **2011**, *3*, 113–116.
16. Taoukil, D.; El bouardi, A.; Sick, F.; Mimet, A.; Ezbakhe, H.; Ajzoul, T. Moisture content influence on the thermal conductivity and diffusivity of wood–concrete composite. *Constr. Build. Mater.* **2013**, *48*, 104–115. [CrossRef]
17. Ahmed, W.; Khushnood, R.A.; Memon, S.A.; Ahmad, S.; Baloch, W.L.; Usman, M. Effective use of sawdust for the production of eco-friendly and thermal-energy efficient normal weight and lightweight concretes with tailored fracture properties. *J. Clean. Prod.* **2018**, *184*, 1016–1027. [CrossRef]
18. Alabduljabbar, H.; Huseien, G.F.; Sam, A.R.M.; Alyouef, R.; Algaifi, H.A.; Alaskar, A. Engineering Properties of Waste Sawdust-Based Lightweight Alkali-Activated Concrete: Experimental Assessment and Numerical Prediction. *Materials* **2020**, *13*, 5490. [CrossRef]
19. Akkaoui, A.; Caré, S.; Vandamme, M. Experimental and micromechanical analysis of the elastic properties of wood-aggregate concrete. *Constr. Build. Mater.* **2017**, *134*, 346–357. [CrossRef]
20. Mnasri, F. Étude du Transfert de Chaleur et de Masse dans les Milieux Complexes: Application aux Milieux Fibreux et à L'isolation des Bâtiments. Ph.D. Thesis, Lorraine University, Lorraine, France, 2016. Available online: [https://theses.hal.science/tel-01508859/file/DDOC\\_T\\_2016\\_0169\\_MNASRI.pdf](https://theses.hal.science/tel-01508859/file/DDOC_T_2016_0169_MNASRI.pdf) (accessed on 8 November 2023).
21. Mnasri, F.; Bahria, S.; Slimani, M.E.-A.; Lahoucine, O.; El Ganaoui, M. Building incorporated bio-based materials: Experimental and numerical study. *J. Build. Eng.* **2020**, *28*, 101088. [CrossRef]
22. Philip, J.R.; De Vries, D.D. Moisture movement in porous materials under temperature gradients. *Eos Trans. Am. Geophys. Union* **1957**, *38*, 222–232.
23. Luikov, A.V. Heat and Mass Transfer in Capillary-Porous Bodies. *Adv. Heat Transf.* **1964**, *1*, 123–184.
24. Künzle, H.M. *Simultaneous Heat and Moisture Transport in Building Components: One- and Two-Dimensional Calculation Using Simple Parameters*; IRB-Verlag: Stuttgart, Germany, 1995.
25. Alioua, T.; Agoudjil, B.; Chennouf, N.; Boudenne, A.; Benzarti, K. Investigation on heat and moisture transfer in bio-based building wall with consideration of the hysteresis effect. *Build. Environ.* **2019**, *163*, 106333. [CrossRef]
26. Belloum, R.; Agoudjil, B.; Chennouf, N.; Boudenne, A. Hygrothermal performance assessment of a bio-based building made with date palm concrete walls. *Build. Environ.* **2022**, *223*, 109467. [CrossRef]
27. Mendes, N.; Ridley, I.; Lamberts, R.; Philippi, P.C.; Budag, K. UMIDUS: A PC program for the prediction of heat and moisture transfer in porous building elements. In Proceedings of the Building Simulation Conference—IBPSA, Kyoto, Japan, 13–15 September 1999; Volume 99, pp. 277–283.
28. Tariku, F.; Kumaran, K.; Fazio, P. Transient model for coupled heat, air and moisture transfer through multilayered porous media. *Int. J. Heat Mass Transf.* **2010**, *53*, 3035–3044. [CrossRef]
29. Qin, M.; Belarbi, R.; Aït-Mokhtar, A.; Nilsson, L.-O. Coupled heat and moisture transfer in multi-layer building materials. *Constr. Build. Mater.* **2009**, *23*, 967–975. [CrossRef]
30. Van Bellegghem, M.; Steeman, M.; Janssen, H.; Janssens, A.; De Paepe, M. Validation of a coupled heat, vapour and liquid moisture transport model for porous materials implemented in CFD. *Build. Environ.* **2014**, *81*, 340–353. [CrossRef]
31. Seng, B.; Lorente, S.; Magniont, C. Scale analysis of heat and moisture transfer through bio-based materials—Application to hemp concrete. *Energy Build.* **2017**, *155*, 546–558. [CrossRef]
32. Ferroukhi, M.Y.; Abahri, K.; Belarbi, R.; Limam, K.; Nouviaire, A. Experimental validation of coupled heat, air and moisture transfer modeling in multilayer building components. *Heat Mass Transf.* **2016**, *52*, 2257–2269. [CrossRef]
33. Benkhaled, M.; Ouldboukhite, S.-E.; Bakkour, A.; Amziane, S. Sensitivity analysis of the parameters for assessing a hygrothermal transfer model HAM in bio-based hemp concrete material. *Int. Commun. Heat Mass Transf.* **2022**, *132*, 105884. [CrossRef]
34. Alioua, T.; Agoudjil, B.; Boudenne, A.; Benzarti, K. Sensitivity analysis of transient heat and moisture transfer in a bio-based date palm concrete wall. *Build. Environ.* **2021**, *202*, 108019. [CrossRef]

35. Othmen, I.; Poullain, P.; Leklou, N. Sensitivity analysis of the transient heat and moisture transfer in a single layer wall. *Eur. J. Environ. Civ. Eng.* **2020**, *24*, 2211–2229. [[CrossRef](#)]
36. Bart, M.; Moissette, S.; Ait Oumeziane, Y.; Lanos, C. Transient hygrothermal modelling of coated hemp-concrete walls. *Eur. J. Environ. Civ. Eng.* **2014**, *18*, 927–944. [[CrossRef](#)]
37. *NF EN 16798-1:2019*; Energy Performance of Buildings—Ventilation for Buildings—Part 1: Indoor Environmental Input Parameters for Design and Assessment of Energy Performance of Buildings Addressing Indoor Air Quality, Thermal Environment, Lighting and Acoustics—Module M1. AFNOR: Paris, France, 2019.
38. Asan, H.; Sancaktar, Y.S. Effects of Wall's thermophysical properties on time lag and decrement factor. *Energy Build.* **1998**, *28*, 159–166. [[CrossRef](#)]
39. Sun, C.; Shu, S.; Ding, G.; Zhang, X.; Hu, X. Investigation of time lags and decrement factors for different building outside temperatures. *Energy Build.* **2013**, *61*, 1–7. [[CrossRef](#)]
40. Hens, H. *Building Physics-Heat, Air and Moisture: Fundamentals and Engineering Methods with Examples and Exercises*, 2nd ed.; John Wiley & Sons: Hoboken, NJ, USA, 2017.
41. COMSOL Multiphysics Reference Manual, Version 5.5, COMSOL AB, Stockholm, Sweden. 2019. Available online: [https://doc.comsol.com/5.5/doc/com.comsol.help.comsol/COMSOL\\_ReferenceManual.pdf](https://doc.comsol.com/5.5/doc/com.comsol.help.comsol/COMSOL_ReferenceManual.pdf) (accessed on 8 November 2023).

**Disclaimer/Publisher's Note:** The statements, opinions and data contained in all publications are solely those of the individual author(s) and contributor(s) and not of MDPI and/or the editor(s). MDPI and/or the editor(s) disclaim responsibility for any injury to people or property resulting from any ideas, methods, instructions or products referred to in the content.